

Online Research @ Cardiff

This is an Open Access document downloaded from ORCA, Cardiff University's institutional repository: <http://orca.cf.ac.uk/102646/>

This is the author's version of a work that was submitted to / accepted for publication.

Citation for final published version:

Pei, Jiajie, Yang, Jiong, Wang, Xibin, Wang, Fan, Mokkaapati, Sudha, Lü, Tieyu, Zheng, Jin-Cheng, Qin, Qinghua, Neshev, Dragomir, Tan, Hark Hoe, Jagadish, Chennupati and Lu, Yuerui 2017. Excited state biexcitons in atomically thin MoSe₂. ACS Nano 11 (7), pp. 7468-7475. 10.1021/acsnano.7b03909 file

Publishers page: <http://dx.doi.org/10.1021/acsnano.7b03909>
<<http://dx.doi.org/10.1021/acsnano.7b03909>>

Please note:

Changes made as a result of publishing processes such as copy-editing, formatting and page numbers may not be reflected in this version. For the definitive version of this publication, please refer to the published source. You are advised to consult the publisher's version if you wish to cite this paper.

This version is being made available in accordance with publisher policies. See <http://orca.cf.ac.uk/policies.html> for usage policies. Copyright and moral rights for publications made available in ORCA are retained by the copyright holders.



Excited State Biexcitons in Atomically Thin MoSe₂

Jiajie Pei,^{1,2†} Jiong Yang,^{1†} Xibin Wang,² Fan Wang,^{3,4} Sudha Mokkaapati,³ Tiejun Lü,⁶ Jincheng Zheng,⁶ Qinghua Qin,¹ Dragomir Neshev,⁵ Hark Hoe Tan,³ Chennupati Jagadish,³ and Yuerui Lu^{1*}

¹Research School of Engineering, College of Engineering and Computer Science, The Australian National University, Canberra, ACT, 2601, Australia

²School of Mechanical Engineering, Beijing Institute of Technology, Beijing, 100081, China

³Department of Electronic Materials Engineering, Research School of Physics and Engineering, The Australian National University, Canberra, ACT, 2601, Australia

⁴ARC Centre for Nanoscale BioPhotonics (CNBP), Department of Physics and Astronomy, Faculty of Science, Macquarie University, Sydney, NSW, 2109, Australia

⁵Nonlinear Physics Centre, Research School of Physics and Engineering, The Australian National University, Canberra, ACT 2601, Australia.

⁶Department of Physics, and Institute of Theoretical Physics and Astrophysics, Xiamen University, Xiamen, 361005, China

† These authors contributed equally to this work

* To whom correspondence should be addressed: Yuerui Lu (yuerui.lu@anu.edu.au)

ABSTRACT

The tightly bound biexcitons found in atomically thin semiconductors have very promising applications for optoelectronic and quantum devices. However, there is a discrepancy between theory and experiment regarding the fundamental structure of these biexcitons. Therefore, the exploration of biexciton formation mechanism by further experiments is of great importance. Here, we successfully triggered the emission of biexcitons in atomically thin MoSe₂, *via* the engineering of three critical parameters: dielectric screening, density of trions and excitation power. The observed binding energy

and formation dynamics of these biexcitons strongly support the model that the biexciton consists of a charge attached to a trion (excited state biexciton) instead of four spatially symmetric particles (ground state biexciton). More importantly, we found the excited state biexcitons can not only exist at cryogenic temperatures, but can also be triggered at room temperature in a freestanding bilayer MoSe₂. The demonstrated capability of biexciton engineering in atomically thin MoSe₂ provides a route for exploring fundamental many-body interactions and enabling device applications, such as bright entangled-photon sources operating at room temperature.

Keywords: MoSe₂, biexciton, two-dimensional materials, freestanding, room temperature

Atomically thin two dimensional (2D) layered transition-metal dichalcogenide (TMD) semiconductors have aroused particular interest because of their unique physical properties and promising implications in both fundamental research and optoelectronic devices.¹⁻⁷ The highly enhanced Coulomb interactions in these atomically thin layers, arising from the reduced dimensionality and weak dielectric screening, allow the formation of tightly bound excitons,⁸ trions^{9, 10} and biexcitons.¹¹⁻¹⁴ Biexcitons have been of particular interest for both fundamental studies of the remarkable many-body interactions¹⁵⁻¹⁷ and investigations of novel device applications, such as quantum logic gates,¹⁸ biexciton lasing devices,^{19, 20} entangled-photon sources,²¹ *etc.* Recently, tightly bound biexcitons have been observed in monolayer TMDs, such as WSe₂,¹¹ MoS₂¹² and WS₂.¹³ These biexcitons in monolayer TMDs show an ultra-large binding energy in the range of 50-70 meV, which is more than one order of magnitude higher than the values found in III-V quasi-2D quantum wells.²² This unique strong binding necessitates the complete understanding of the structures of these biexcitons and their dynamics in 2D materials, as well as to characterize their properties and fully investigate their potential functionalities. A few theoretical models, such as the path integral Monte Carlo approach,²³

effective mass model²⁴ and variational calculation method,¹¹ have been used to estimate the binding energies of biexcitons in TMD 2D materials. These models consider a biexciton to be a spatially symmetric four-particle state. However, based on this symmetric four-particle model, the predicted binding energies of biexcitons in TMD monolayers^{11, 23-25} are in the range of 18-24 meV, less than half of the values observed,¹¹⁻¹³ suggesting a discrepancy between theory and experiment. Recently, Varga *et al.*,²⁵ using high-accuracy variational calculations, showed that the predicted binding energies of excited state biexcitons in TMD monolayers are in the range of 50-70 meV, which agrees well with the earlier experimental data.¹¹⁻¹³ In Varga's model,²⁵ the excited state biexciton corresponds to a charge attached to a trion, which is energetically favorable than the ground state biexciton consisting of four spatially symmetric particles. How to further experimentally confirm the existence of the trion-charge bound excited state biexcitons in the Varga's model is extremely important. This will allow us to fully understand the structures and formation mechanisms of these biexcitons and will enable us to overcome the limitations of previous experiments by engineering the environment of these biexcitons.

RESULTS/DISCUSSION

Here, we successfully observed tightly bound biexcitons with a binding energy of ~60 meV in atomically thin MoSe₂. The measured binding energy matches well with the theoretically predicted value of the excited state biexcitons in MoSe₂.²⁵ We further probed the formation dynamics of these biexcitons and found that the density of biexcitons increases with increasing density of negative trions and decreases with increasing density of excitons. This finding suggests that the biexcitons observed here are excited state biexcitons, instead of ground state biexcitons. More importantly, we successfully triggered the emission of excited state biexcitons at room temperature in a freestanding bilayer MoSe₂ by modulating three independent parameters: 1) dielectric screening; 2) density of trions; 3) excitation power. The implications

of the tightly bound biexcitons at room temperature in 2D materials are far-reaching. It provides a room-temperature 2D platform to explore fundamental many-body interactions, which provides a route for quantum logical devices and entangled-photon sources operating at room temperature.

It has been known that many-body effects,^{26, 27} which determine the behaviors of excitons, trions, and biexcitons, play important roles in optical transitions in low dimensional materials, including quantum wells, carbon nanotubes, 2D semiconductors and so on.^{8, 11, 26-37} Such a many-body effect, arising mainly from strong Coulomb interactions among charges, can be significantly enhanced with the reduction of dielectric screening from the environment^{11, 26, 27, 38} (Figures 1a and 1b). Thus, the biexciton or even higher-order multiple-exciton states will typically become more pronounced in an environment with lower dielectric screening. To explore the dielectric screening effect on the many-body interactions in atomically thin semiconductors, we fabricated two types of MoSe₂ samples: SiO₂-supported and freestanding thin layers. The freestanding MoSe₂ sample was fabricated by mechanically transferring the sample onto a pre-patterned circular hole on a SiO₂/Si substrate, as illustrated in Figure 1c. The freestanding atomically thin layers were confirmed by the contrast difference in optical microscope images (Figure 1d and Figure S1a) and the photoluminescence (PL) intensity difference in the PL mapping images (Figure 1e and Figure S1b). The layer number was identified and confirmed by phase-shifting interferometry³⁹ and PL spectroscopy measurements.

We compared the PL spectra of the MoSe₂ samples measured at 6 K and found that for the SiO₂-supported bilayer (2L) and monolayer (1L) MoSe₂ samples, there are only two distinct PL peaks at approximately 1.615 and 1.645 eV (Figure 1f and Figure S1c). These PL peaks can be identified as trion (T) and exciton (A) peaks, respectively, according to previous

studies.¹⁰ Importantly, a new PL emission peak “X”, at approximately 1.585 eV was observed from both the freestanding 2L (Figure 1f) and 1L (Figure S1d) MoSe₂ samples. We observed this new peak from multiple freestanding 1L and 2L MoSe₂ samples (more than 3 samples for each type). For some freestanding 2L MoSe₂ samples, this new peak became completely dominant in the PL spectrum, and the exciton (A) and trion (T) peaks were not pronounced at 6 K (Figure 2 and Figure S3), possibly because these samples had slightly different sample-dependent initial doping levels compared with the one shown in Figure 1f.

To determine the origin of this new peak X, we carried out power-dependent PL measurements on one freestanding 2L MoSe₂ sample at 6 K (Figure 2a). For a quantitative analysis, the integrated PL intensity of the X peak was plotted as a function of that of the exciton (A) peak (Figure 2b). By fitting the data with a power-law $I_X \propto I_A^\alpha$, where I_X is the integrated PL intensity of X peak and I_A is the integrated PL intensity of A peak,¹¹ it is found that peak X grows super-linearly with the excitation power ($\alpha \sim 1.23$). Based on the measured α value, peak X is attributed to the emission of biexcitons. In the ideal case, the α value of biexciton emission is expected to be close to 2; however, α values in the range of 1.2 to 1.9 were typically observed for biexciton emissions in quantum well systems^{40,41} and TMD semiconductors^{11,14} that might be due to the lack of thermal equilibrium between the states.¹¹

Time-resolved PL (TRPL) measurement is another useful approach to identify the emission features in a PL spectrum. We measured the TRPL traces for the peaks A, T, and X (Figure 2c) at temperature 6 K. The decay trace curves were deconvoluted with respect to the instrument response and then were fitted with the equation $I = A \exp\left(-\frac{t}{\tau_1}\right) + B \exp\left(-\frac{t}{\tau_2}\right) + C$, where I is the PL intensity, A , B and C are constants, t is time, and τ_1 is faster decay rate and τ_2 is the slower decay rate indicating emission lifetimes for different decay processes.⁴² The measured lifetimes of exciton (A), trion (T) and biexciton (X) were on the same order and comparable

with each other, which is consistent with what has been reported in monolayer WSe₂,¹¹ indicating that the peak X is indeed from biexciton rather than localized exciton, since the lifetime of localized exciton should be an order longer than exciton and trion.¹¹ Moreover, the peaks A, T, X from the freestanding 1L MoSe₂ sample (Figure S4) possess consistent lifetimes with the respective peaks in freestanding 2L MoSe₂ (Figure 2d), which suggests the same emission features in both freestanding 1L and 2L MoSe₂ samples.

In addition, the spectrum of this new emission feature is asymmetric and can be fitted to two peaks, labelled as “X” and “L”, by Lorentzian fitting (Figure S1d and Figure S2). The peak X is from the biexciton emission as discussed above, while the lower energy peak L could be from the contribution of defect states and is not the focus of this work. The measured full width at half maximum (FWHM) value of the biexciton peak X in both freestanding 1L and 2L MoSe₂ samples was ~46 meV, which is similar to that of the biexciton peak observed in 1L WS₂.¹⁴ From the temperature-dependent PL measurements (Figure S3a), we can clearly see that the intensity of the X peak increased dramatically as the temperature decreased from 63 to 6 K (Figure S3c).

Taken together, the observed power dependence and temporal dynamics properties of the X feature provide strong evidence for its assignment as a biexciton feature. We thus explored the binding energy of biexcitons and their dynamics to obtain a deeper physical insight into the biexcitons in atomically thin MoSe₂ layers. The binding energy of biexcitons is given by the energy difference between the exciton and biexciton peaks, assuming that an exciton is produced in the radiative decay of a biexciton.¹¹ The measured energy difference values between the X and A peaks in freestanding 1L and 2L MoSe₂ samples are 60 meV (Fig S1d) and 57 meV (Fig S2), respectively, which are considered to be the biexciton binding energies of MoSe₂. These values match very well with the calculated binding energy (58 meV) of an

excited state biexciton in MoSe₂²⁵ (see Table 1). Freestanding 2L MoSe₂ has slightly smaller biexciton binding energy than 1L MoSe₂, which might be due to the relatively larger screening in 2L MoSe₂. According to the theoretical model,²⁵ an excited state biexciton consists of a charge attached to a trion. The formation of an excited state biexciton state (*TC*) can be denoted as $T + C \rightarrow TC$, where *T* is a trion and *C* is a charge. In great contrast, the calculated binding energy of a ground state biexciton (spatially symmetric exciton pairs, denoted as $A + A \rightarrow AA$) in MoSe₂ is only 18 meV (Table 1), which is much smaller than the observed biexciton binding energy.

In addition to the binding energy difference, another way to differentiate the excited state and ground state biexcitons is to probe the dynamic relationship between the densities of biexcitons and trions. Based on the different formation mechanisms of these biexcitons, the density of excited state biexcitons should increase with the increase of trion density, whereas the density of ground state biexcitons should decrease because the formation of trions can reduce the density of excitons. Here, we successfully used an electrostatic doping technique to control the trion density in a 2L MoSe₂ metal-oxide-semiconductor (MOS) device (Figure S5) at 83 K, which leads to the dynamic modulation of biexciton emission (Figure 3).

Firstly, we carried out the PL intensity mapping as a function of photon energy and gate voltage, using a relatively low excitation power of 264 μ W (Figure 3a). Under a back gate voltage of 50 V, the negative trion (T) emission peak was dominant in the PL spectrum. At the same time, a new PL peak (labelled as X) at the low energy side showed up. When a negative back gate voltage of -50 V was applied, the exciton (A) emission peak became dominant and the new PL peak X disappeared (Figure 3a and 3c). To obtain a better insight, we generated the PL intensity mapping again using a relatively high excitation power of 602 μ W (Figure 3b). The intensity of this new PL peak X increased much faster than the intensities of the exciton and trion peaks.

Based on the super-linear increasing manner, this new PL peak X is assigned to the emission of biexcitons. From Figures 3b and 3d, we can clearly see that the density of biexcitons increases with increasing density of negative trions and decreases with increasing density of excitons. This further confirms that biexcitons observed here are excited state biexcitons (Figure 3e), instead of ground state biexcitons (Figure 3f). According to the calculation results by Varga *et al.*,²⁵ the binding energy of ground state biexcitons is only 18 meV, very close to the binding energy of trions. Therefore, it might not be possible to distinguish the ground state biexcitons and trions in experiments.²⁵ Also, excited state biexcitons are more likely to be observed in experiments than ground state biexcitons, since excited state biexcitons are energetically favorable and are spatially extended.²⁵ In addition, we only observed the emissions of excitons and trions, but no emission of biexcitons, in 1L MoSe₂ MOS devices at 83 K (Figure S6), which is consistent with previous report.¹⁰ The different PL behaviors in 2L and 1L MoSe₂ MOS devices are likely caused by the different trion densities in 2L and 1L MoSe₂ samples (as will be discussed later).

Due to thermally activated dissociation, biexcitons in both the freestanding MoSe₂ samples (Figure 1) and the 2L MoSe₂ MOS device (Figure 3) could only be observed at cryogenic temperatures ($T < 100$ K), which is similar to previously reported biexcitons in other TMD semiconductors.¹¹⁻¹⁴ The requirement of cryogenic temperature would significantly limit the potential applications of biexcitons. Fortunately, our experimental data (Figure 1-3) have shown that the probability of biexciton emissions in atomically thin MoSe₂ can be enhanced under the following three conditions (Figure 4a): 1) reduced dielectric screening; 2) enhanced density of trion states; 3) high excitation laser power.

Here, we successfully demonstrated the emission of excited state biexcitons at room temperature in freestanding 2L MoSe₂ samples, in which those three parameters were all well

optimized (Figure 4). To achieve a clear comparison, we measured PL intensity mapping plots at room temperature as a function of photon energy and excitation power for four types of MoSe₂ systems (Figure 4b-e): freestanding 2L, freestanding 1L, SiO₂-supported 2L and SiO₂-supported 1L. A biexciton emission feature at ~1.490 eV was observed only in the freestanding 2L MoSe₂ sample under relatively high excitation power at room temperature. To confirm the assignment of the biexciton peak in Figure 4b, we fitted the PL spectra and plotted the integrated intensities of the trion and biexciton peaks as a function of excitation power, as shown in Figure S7. At low excitation power, the trion peak (T) was dominant in the PL spectrum. With the growth of excitation power, however the intensity of the X peak increased much faster than that of the trion peak. Particularly, when the excitation power was lower than 50 μ W, the integrated intensity of the trion and biexciton peaks increased as a function of power with exponent (α) values of ~0.85 and ~1.01, respectively. When the excitation power was higher than 50 μ W, the X peak became dominant in the PL spectrum, and the α -values of the trion and biexciton peaks became ~0.55 and ~1.41, respectively. The super-linear power dependence of this X peak further confirms its biexciton assignment. At high excitation power, the α -value of the trion peak decreases, while that of the biexciton peak increases, which suggests the conversion of the trions to excited state biexcitons. In addition, the α value of the trion peak at room temperature was slightly less than 1, similar to the situation observed in other TMD semiconductors^{11,14} due to the lack of full equilibrium.⁸ On the other hand, the ratio of α values between biexciton and trion (1.41/0.55) increases dramatically when the excitation power is higher than 50 μ W, suggesting that there might be a threshold value of trion density. Before the threshold, the transformation from trion to biexciton is restrained to some extent; beyond the threshold, the transformation from trion to biexciton start to dominate. In the power-dependent PL measurements, we used relatively low pumping power and the power-induced spectral shifts of the exciton peaks in all freestanding and SiO₂-supported samples were less

than 2.9 meV (Figures 4c, 4e, 3c and 3d), similar to the situation in a previous report.¹¹ This suggests that our pump laser has negligible heating effect on all the samples. The band gap renormalization effect can be ignored in Figure 4b, owing to the relatively low photo-doping level (Supplementary Information).

The reason why biexciton is observed in freestanding 2L instead of 1L MoSe₂ at room temperature could be explained as follows. 1L MoSe₂ gives only one PL peak at ~1.562 eV from the emission of excitons at room temperature, while 2L MoSe₂ gives only one PL peak at ~1.520 eV from the emission of trions, which can be clearly observed from their temperature-dependent PL measurements (Figure S8a and S8b). This difference might be caused by the relatively low initial doping levels in MoSe₂ crystals¹⁰ and the different band gap natures in 1L and 2L MoSe₂ samples. 1L MoSe₂ possesses a direct band gap, and thus a relatively balanced distribution of thermal charges in the K-K valleys of the band structure, where the PL transitions occur. In contrast, 2L MoSe₂ possesses an indirect band gap and thus an un-balanced thermal charge distribution in the K-K valleys, which leads to a higher trion density (Figure S8c and S8d). Therefore, at room temperature, a freestanding 2L MoSe₂ sample possesses low dielectric screening and high trion density, which leads to the emission of excited state biexcitons under a relatively high excitation power. The demonstrated capability of biexciton engineering at room temperature in MoSe₂ will allow us to explore fundamental many-body interactions in a simplified room-temperature 2D platform, which will enable a class of quantum devices, such as bright entangled and correlated photon sources operating at room temperature.²¹ In addition, based on theoretical calculations, biexcitons have larger radius than excitons and trions in 2D TMDs (Supplementary Information). Because of the larger separation between charges in biexcitons, the Coulomb interactions of biexcitons are more likely to be influenced by dielectric screening of the external media than those of trions in TMDs.¹¹

CONCLUSIONS

In conclusion, we observed tightly bound excited state biexcitons with a binding energy of ~ 60 meV in atomically thin MoSe₂, which was confirmed by both the agreement of experimental and theoretical values of the binding energy and the observed formation dynamics of these excited state biexcitons. We also found that the emission from these excited state biexcitons in atomically thin MoSe₂ strongly relies on three important conditions: reduced dielectric screening, high density of trions and high excitation power. By optimizing those three conditions, we successfully triggered the emission of excited state biexcitons in freestanding 2L MoSe₂ samples at room temperature. Our findings will provide a platform to explore fundamental many-body interactions in atomically thin semiconductors. We envisage that such 2D platform can form the bases of bright quantum sources of entangled and correlated photons, thus enabling a class of ultrafast optoelectronics and quantum devices with applications in quantum communications and cryptography.

METHODS/EXPERIMENTAL

Device Fabrication and Characterization. Mechanical exfoliation was used to drily transfer 1L and 2L MoSe₂ flakes onto the SiO₂/Si substrate (a 275-nm layer of thermal oxide on n⁺-doped silicon), near the pre-patterned Au electrode for those MOS devices. The Au electrodes were patterned by conventional photolithography, metal deposition, and lift-off processes. Another thick graphite flake was similarly transferred to electrically bridge the MoSe₂ flake and the Au electrode, forming a MOS device. For the suspended samples, 1L and 2L MoSe₂ samples were drily transferred onto a 275 nm SiO₂/Si substrate with pre-etched 3 μm-deep holes.

Optical Characterizations. PL measurements at room temperature and 83 K were conducted using a Horiba JobinYvon T64000 micro-Raman system equipped with charge-coupled device (CCD) and InGaAs detectors, along with a 532 nm Nd:YAG laser as the excitation source. For low temperature (down to 83 K) measurements, the sample was placed into a microscope-compatible chamber with a low temperature controller (using liquid nitrogen as the coolant). Micro-PL spatial mapping was performed using a commercial WiTec alpha300S system in the scanning confocal microscope configuration. The power-dependent PL measurements at 6 K and TRPL measurements were conducted in a setup that incorporates micro-PL spectroscopy with a time-correlated single photon counting (TCSPC) system and uses liquid helium as the coolant. A linearly polarized pulsed laser (frequency doubled to 522 nm, with a 300 fs pulse width and a 20.8 MHz repetition rate) was directed to a high numerical aperture (NA = 0.7) objective (Nikon S Plan 60x). The PL signal was collected by a grating spectrometer, thereby either recording the PL spectrum through the CCD (Princeton Instruments, PIXIS) or detecting the PL intensity decay by a Si single photon avalanche diode (SPAD) and the TCSPC (PicoHarp 300) system with a resolution of 20 ps. All the PL spectra were corrected for the

instrument response. Electrical bias was applied using a Keithley 4200 semiconductor analyzer.

Simulations. First-principle calculations based on the density functional theory (DFT) were used to calculate band diagrams of 1L and 2L MoSe₂. The scissor operator was used to correct the band gaps to GW approximation (GWA) values.

ASSOCIATED CONTENT

Supporting Information

The Supporting Information is available free of charge on the ACS Publications website at DOI: 00.0000/acsnano.0000000. Details of more experimental PL measurement results and data analysis (PDF).

AUTHOR CONTRIBUTIONS

Y. R. L. designed the project; J. J. P. carried out sample mechanical exfoliation and microscope imaging; J. Y. and J. J. P. carried out the PL measurements; F. W., S. M, H. T. and C. J. built the set up for PL measurements; D. N. built the set up for micro-PL mapping; T. Y. L and J. C. Z. conducted the DFT calculations; J. J. P., Y. R. L, and J. Y. analyzed the data and prepared the manuscript; all authors contributed to the manuscript.

ACKNOWLEDGEMENTS

We would like to acknowledge the facility support from the ACT node of the Australian National Fabrication Facility (ANFF). We also acknowledge financial support from ANU PhD student scholarship, China Scholarship Council, Australian Research Council, ANU Major Equipment Committee fund (No.: 14MEC34), ARC Discovery early career researcher award (DECRA) DE140100805, National Natural Science Foundation of China, the Fundamental Research Funds for Central Universities, the Natural Science Foundation of Fujian Province, China, Special Program for Applied Research on Super Computation of the NSFC-Guangdong

Joint Fund.

Competing financial interests

The authors declare that they have no competing financial interests.

FIGURE CAPTIONS

Figure 1. Photoluminescence (PL) of freestanding and dielectric-supported atomically thin MoSe₂. (a-b), Schematic representation of excitons (bound electron-hole pairs) for the freestanding (a) and dielectric-supported (b) monolayers. (c), Schematic cross section view of the device with freestanding MoSe₂. The MoSe₂ sample was mechanically transferred across circular holes that were pre-patterned on a SiO₂ (275 nm)/Si substrate. The depth of the holes is 3 μm. (d), Optical microscope image of the freestanding bilayer (2L) MoSe₂ samples across 6 μm-diameter holes. (e), PL mapping image of the region marked by the dashed square in (d). The holes covered by the freestanding sample are bright, while the holes without samples are dark. (f), Measured PL spectra from freestanding (red line) and SiO₂-supported (black line) 2L MoSe₂ at 6 K. The labels “A,” “T” and “X” represent the emissions from excitons, trions and a new emission peak, respectively.

Figure 2. Power-dependent and time-resolved PL characterization. (a), Measured PL spectra from freestanding area (red lines) and SiO₂ supported area (black lines) under various excitation powers. (b), Log-log plot of integrated PL intensity of the peak X as a function of that of peak A. From the fitting curve, integrated PL intensity of the X peak grows super-linearly ($\alpha \sim 1.23$), with the increase of excitation power. (c), Measured time-resolved PL traces for A, T, and X peaks at temperature of 6 K. IR represents instrument response curve. Based on the deconvolution with respect to the instrument response and a double exponential fit using the equation $I = A \exp\left(-\frac{t}{\tau_1}\right) + B \exp\left(-\frac{t}{\tau_2}\right) + C$, the fast decay lifetime τ_1 (and the corresponding amplitude A) values of exciton (A), trion (T), and biexciton (X) were extracted to be 8.7 (0.992), 9.8 (0.992), and 9.1 (0.988) ps, respectively; the slow decay lifetime τ_2 (and the corresponding amplitude B) values of exciton (A), trion (T), and biexciton (X) were extracted to be 292.8 (0.008), 322.6 (0.008), and 477.5 (0.012) ps, respectively.

Figure 3. Electrostatic control of biexciton emissions. (a-b), PL intensity mapping as a function of photon energy and gate voltage from a 2L MoSe₂ metal-oxide-semiconductor (MOS) device measured at 83 K under different excitation power values of 264 (a) and 602 μW (b). Distinct exciton peaks show up as the back gate voltage goes from +50 V to -50 V, indicating trions in the bilayer MoSe₂ sample are negatively charged. (c-d), Measured PL spectra (gray lines) from the 2L MoSe₂ MOS device shown in a and b, respectively, under gate voltages of 50 and -50 V. The PL spectra are fitted to Lorentzian peaks, labeled as “X,” (red

line) “T” (blue line) and “A” (black line). Purple lines are the cumulative fitting results. (e-f), Schematic plots showing the formation process of excited state (e) and ground state biexcitons (f).

Figure 4. Excited state biexciton engineering at room temperature in atomically thin MoSe₂. (a), Schematic plots showing that the density of excited state biexciton will be enhanced with lower dielectric screening, higher density of trions, and higher excitation power. (b-e), Measured PL intensity mapping plots at room temperature as a function of photon energy and excitation power for four types of MoSe₂ samples: freestanding 2L (b), freestanding 1L (c), SiO₂-supported 2L and (d), SiO₂-supported 1L.

REFERENCES

1. Britnell, L.; Ribeiro, R. M.; Eckmann, A.; Jalil, R.; Belle, B. D.; Mishchenko, A.; Kim, Y.-J.; Gorbachev, R. V.; Georgiou, T.; Morozov, S. V.; Grigorenko, A. N.; Geim, A. K.; Casiraghi, C.; Neto, A. H. C.; Novoselov, K. S. Strong Light-Matter Interactions in Heterostructures of Atomically Thin Films. *Science* **2013**, *340*, 1311-1314.
2. Yang, J.; Wang, Z.; Wang, F.; Xu, R.; Tao, J.; Zhang, S.; Qin, Q.; Luther-Davies, B.; Jagadish, C.; Yu, Z.; Lu, Y. Atomically Thin Optical Lenses and Gratings. *Light Sci. Appl.* **2016**, *5*, e16046.
3. Lopez-Sanchez, O.; Lembke, D.; Kayci, M.; Radenovic, A.; Kis, A. Ultrasensitive Photodetectors Based on Monolayer MoS₂. *Nat. Nanotechnol.* **2013**, *8*, 497-501.
4. Ye, Y.; Wong, Z. J.; Lu, X.; Ni, X.; Zhu, H.; Chen, X.; Wang, Y.; Zhang, X. Monolayer Excitonic Laser. *Nat. Photonics* **2015**, *9*, 733-737.
5. Chen, H.; Corboliou, V.; Solntsev, A. S.; Choi, D.-Y.; Vincenti, M. A.; de Ceglia, D.; De Angelis, C.; Lu, Y.; Neshev, D. N. Enhanced Second-Harmonic Generation from Two-Dimensional MoSe₂ on a Silicon Waveguide. *Light Sci. Appl.* **2017**, *6*, e17060.
6. Chen, H.; Yang, J.; Rusak, E.; Straubel, J.; Guo, R.; Myint, Y. W.; Pei, J.; Decker, M.; Staude, I.; Rockstuhl, C.; Lu, Y.; Kivshar, Y. S.; Neshev, D. Manipulation of Photoluminescence of Two-Dimensional MoSe₂ by Gold Nanoantennas. *Sci. Rep.* **2016**, *6*, 22296.
7. Zhu, Y.; Yang, J.; Zhang, S.; Mokhtar, S.; Pei, J.; Wang, X.; Lu, Y. Strongly Enhanced Photoluminescence in Nanostructured Monolayer MoS₂ by Chemical Vapor Deposition. *Nanotechnology* **2016**, *27*, 135706.
8. He, K.; Kumar, N.; Zhao, L.; Wang, Z.; Mak, K. F.; Zhao, H.; Shan, J. Tightly Bound Excitons in Monolayer WSe₂. *Phys. Rev. Lett.* **2014**, *113*, 026803.
9. Mak, K. F.; He, K.; Lee, C.; Lee, G. H.; Hone, J.; Heinz, T. F.; Shan, J. Tightly Bound Trions in Monolayer MoS₂. *Nat. Mater.* **2013**, *12*, 207-211.
10. Ross, J. S.; Wu, S.; Yu, H.; Ghimire, N. J.; Jones, A. M.; Aivazian, G.; Yan, J.; Mandrus, D. G.; Xiao, D.; Yao, W.; Xu, X. Electrical Control of Neutral and Charged Excitons in a Monolayer Semiconductor. *Nat. Commun.* **2013**, *4*, 1474.
11. You, Y.; Zhang, X.-X.; Berkelbach, T. C.; Hybertsen, M. S.; Reichman, D. R.; Heinz, T. F. Observation of Biexcitons in Monolayer WSe₂. *Nat. Phys.* **2015**, *11*, 477-481.
12. Mai, C.; Barrette, A.; Yu, Y.; Semenov, Y. G.; Kim, K. W.; Cao, L.; Gundogdu, K. Many-Body Effects in Valleytronics: Direct Measurement of Valley Lifetimes in Single-Layer MoS₂. *Nano Lett.* **2014**, *14*, 202-206.
13. Plechinger, G.; Nagler, P.; Kraus, J.; Paradiso, N.; Strunk, C.; Schüller, C.; Korn, T. Identification of Excitons, Trions and Biexcitons in Single-Layer WS₂. *Phys. Status Solidi RRL* **2015**, *9*, 457-461.
14. Shang, J.; Shen, X.; Cong, C.; Peimyoo, N.; Cao, B.; Eginligil, M.; Yu, T. Observation of Excitonic Fine Structure in a 2D Transition-Metal Dichalcogenide Semiconductor. *ACS Nano* **2015**, *9*, 647-655.
15. Soavi, G.; Dal Conte, S.; Manzoni, C.; Viola, D.; Narita, A.; Hu, Y.; Feng, X.; Hohenester, U.; Molinari, E.; Prezzi, D.; Mullen, K.; Cerullo, G. Exciton-Exciton Annihilation and Biexciton Stimulated Emission in Graphene Nanoribbons. *Nat. Commun.* **2016**, *7*.
16. Chen, G.; Stievater, T. H.; Batteh, E. T.; Li, X.; Steel, D. G.; Gammon, D.; Katzer, D. S.; Park, D.; Sham, L. J. Biexciton Quantum Coherence in a Single Quantum Dot. *Phys. Rev. Lett.* **2002**, *88*, 117901.
17. Pedersen, T. G.; Pedersen, K.; Cornean, H. D.; Duclos, P. Stability and Signatures of Biexcitons in Carbon Nanotubes. *Nano Lett.* **2005**, *5*, 291-294.

18. Li, X.; Wu, Y.; Steel, D.; Gammon, D.; Stievater, T. H.; Katzer, D. S.; Park, D.; Piermarocchi, C.; Sham, L. J. An All-Optical Quantum Gate in a Semiconductor Quantum Dot. *Science* **2003**, 301, 809-811.
19. Grim, J. Q.; Christodoulou, S.; Di Stasio, F.; Krahne, R.; Cingolani, R.; Manna, L.; Moreels, I. Continuous-Wave Biexciton Lasing at Room Temperature Using Solution-Processed Quantum Wells. *Nat. Nanotechnol.* **2014**, 9, 891-895.
20. Masumoto, Y.; Kawamura, T.; Era, K. Biexciton Lasing in CuCl Quantum Dots. *Appl. Phys. Lett.* **1993**, 62, 225-227.
21. Shields, A. J. Semiconductor Quantum Light Sources. *Nat. Photonics* **2007**, 1, 215-223.
22. Klingshirn, C. F. *Semiconductor Optics*. Springer: **2007**; Vol. 3.
23. Velizhanin, K. A.; Saxena, A. Excitonic Effects in Two-Dimensional Semiconductors: Path Integral Monte Carlo Approach. *Phys. Rev. B* **2015**, 92, 195305.
24. Riva, C.; Peeters, F. M.; Varga, K. Excitons and Charged Excitons in Semiconductor Quantum Wells. *Phys. Rev. B* **2000**, 61, 13873-13881.
25. Zhang, D. K.; Kidd, D. W.; Varga, K. Excited Biexcitons in Transition Metal Dichalcogenides. *Nano Lett.* **2015**, 15, 7002-7005.
26. Qiu, D. Y.; da Jornada, F. H.; Louie, S. G. Optical Spectrum of MoS₂: Many-Body Effects and Diversity of Exciton States. *Phys. Rev. Lett.* **2013**, 111, 216805.
27. Molina-Sánchez, A.; Sangalli, D.; Hummer, K.; Marini, A.; Wirtz, L. Effect of Spin-Orbit Interaction on the Optical Spectra of Single-Layer, Double-Layer, and Bulk MoS₂. *Phys. Rev. B* **2013**, 88, 045412.
28. Perebeinos, V.; Tersoff, J.; Avouris, P. Scaling of Excitons in Carbon Nanotubes. *Phys. Rev. Lett.* **2004**, 92, 257402.
29. Kulik, L. V.; Kulakovskii, V. D.; Bayer, M.; Forchel, A.; Gippius, N. A.; Tikhodeev, S. G. Dielectric Enhancement of Excitons in near-Surface Quantum Wells. *Phys. Rev. B* **1996**, 54, R2335-R2338.
30. Yang, J.; Lü, T.; Myint, Y. W.; Pei, J.; Macdonald, D.; Zheng, J.-C.; Lu, Y. Robust Excitons and Trions in Monolayer MoTe₂. *ACS Nano* **2015**, 9, 6603-6609.
31. Xu, R.; Yang, J.; Myint, Y. W.; Pei, J.; Yan, H.; Wang, F.; Lu, Y. Exciton Brightening in Monolayer Phosphorene via Dimensionality Modification. *Adv. Mater.* **2016**, 28, 3493-3498.
32. Xu, R.; Zhang, S.; Wang, F.; Yang, J.; Wang, Z.; Pei, J.; Myint, Y. W.; Xing, B.; Yu, Z.; Fu, L.; Qin, Q.; Lu, Y. Extraordinarily Bound Quasi-One-Dimensional Trions in Two-Dimensional Phosphorene Atomic Semiconductors. *ACS Nano* **2016**, 10, 2046-2053.
33. Zhang, S.; Yang, J.; Xu, R.; Wang, F.; Li, W.; Ghufuran, M.; Zhang, Y.-W.; Yu, Z.; Zhang, G.; Qin, Q.; Lu, Y. Extraordinary Photoluminescence and Strong Temperature/Angle-Dependent Raman Responses in Few-Layer Phosphorene. *ACS Nano* **2014**, 8, 9590-9596.
34. Xu, R.; Yang, J.; Zhu, Y.; Yan, H.; Pei, J.; Myint, Y. W.; Zhang, S.; Lu, Y. Layer-Dependent Surface Potential of Phosphorene and Anisotropic/Layer-Dependent Charge Transfer in Phosphorene-Gold Hybrid Systems. *Nanoscale* **2016**, 8, 129-135.
35. Lu, J.; Yang, J.; Carvalho, A.; Liu, H.; Lu, Y.; Sow, C. H. Light-Matter Interactions in Phosphorene. *Acc. Chem. Res.* **2016**, 49, 1806-1815.
36. Pei, J.; Gai, X.; Yang, J.; Wang, X.; Yu, Z.; Choi, D.-Y.; Luther-Davies, B.; Lu, Y. Producing Air-Stable Monolayers of Phosphorene and Their Defect Engineering. *Nat. Commun.* **2016**, 7, 10450.
37. Pei, J.; Yang, J.; Xu, R.; Zeng, Y.-H.; Myint, Y. W.; Zhang, S.; Zheng, J.-C.; Qin, Q.; Wang, X.; Jiang, W.; Lu, Y. Exciton and Trion Dynamics in Bilayer MoS₂. *Small* **2015**, 11, 6384-6390.

38. Lin, Y.; Ling, X.; Yu, L.; Huang, S.; Hsu, A. L.; Lee, Y.-H.; Kong, J.; Dresselhaus, M. S.; Palacios, T. Dielectric Screening of Excitons and Trions in Single-Layer MoS₂. *Nano Lett.* **2014**, 14, 5569-5576.
39. Yang, J.; Xu, R. J.; Pei, J. J.; Myint, Y. W.; Wang, F.; Wang, Z.; Zhang, S.; Yu, Z. F.; Lu, Y. R. Optical Tuning of Exciton and Trion Emissions in Monolayer Phosphorene. *Light Sci. Appl.* **2015**, 4, e312.
40. Phillips, R. T.; Lovering, D. J.; Denton, G. J.; Smith, G. W. Biexciton Creation and Recombination in a GaAs Quantum Well. *Phys. Rev. B* **1992**, 45, 4308-4311.
41. Birkedal, D.; Singh, J.; Lyssenko, V. G.; Erland, J.; Hvam, J. M. Binding of Quasi-Two-Dimensional Biexcitons. *Phys. Rev. Lett.* **1996**, 76, 672-675.
42. Xuefeng, L.; Hongyi, Y.; Qingqing, J.; Zhihan, G.; Shaofeng, G.; Jun, Q.; Zhongfan, L.; Yanfeng, Z.; Dong, S. An Ultrafast Terahertz Probe of the Transient Evolution of the Charged and Neutral Phase of Photo-Excited Electron-Hole Gas in a Monolayer Semiconductor. *2D Mater.* **2016**, 3, 014001.

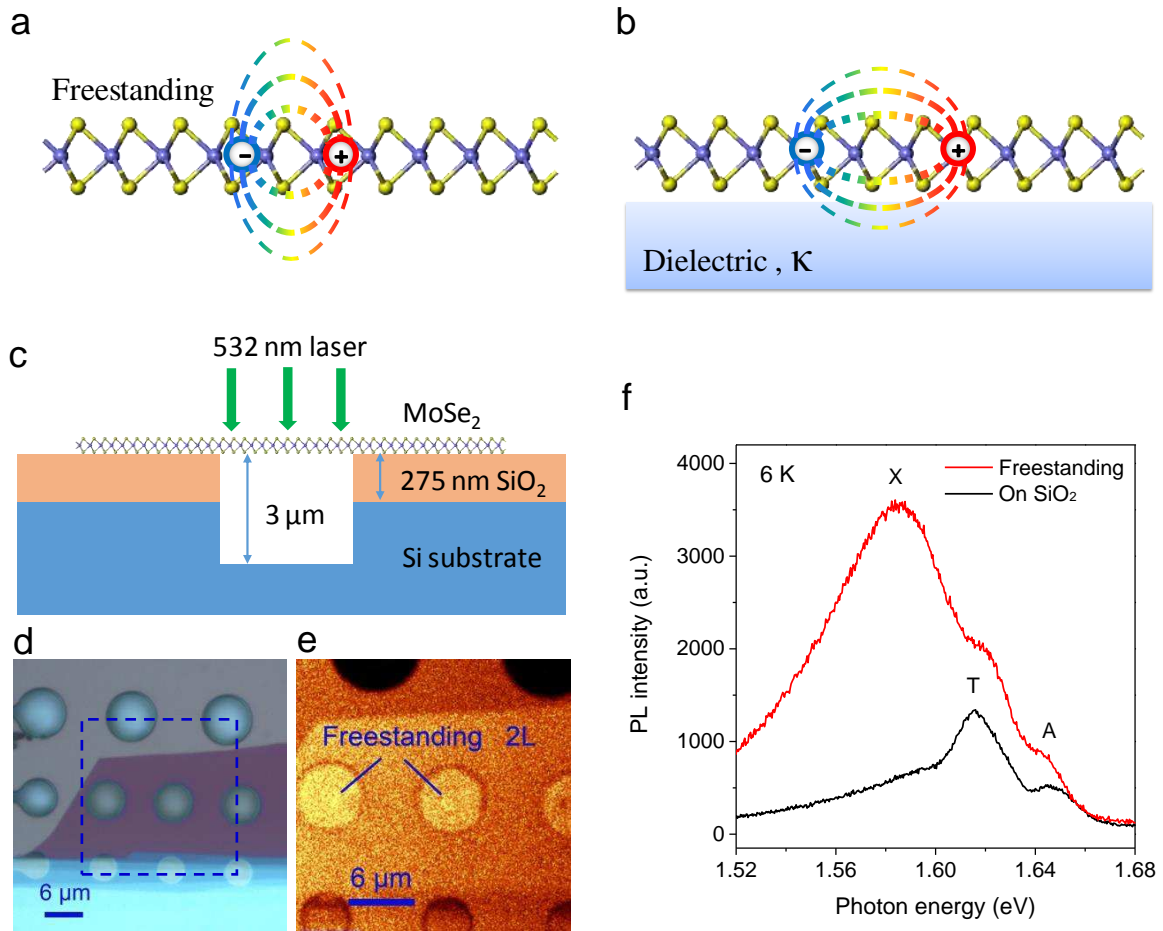


Figure 1

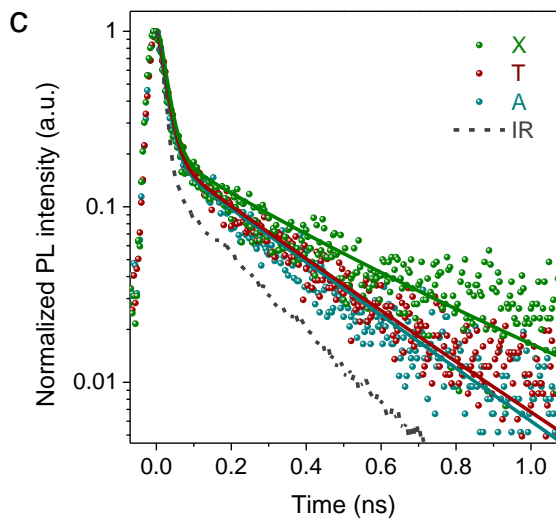
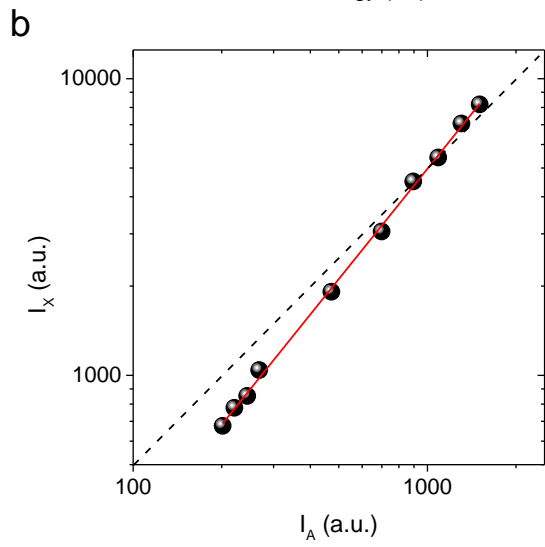
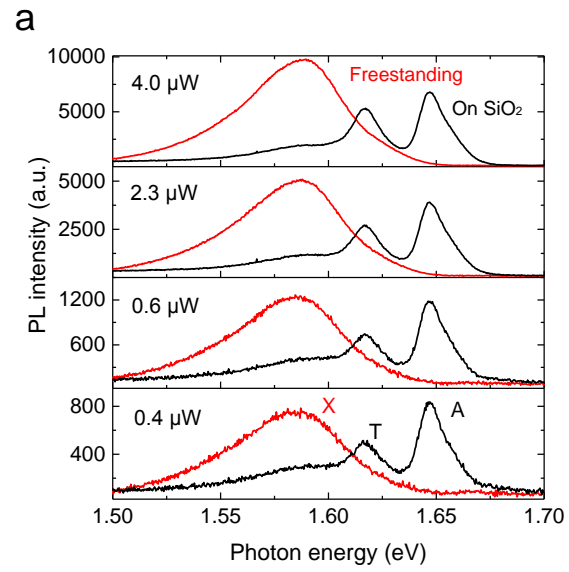


Figure 2

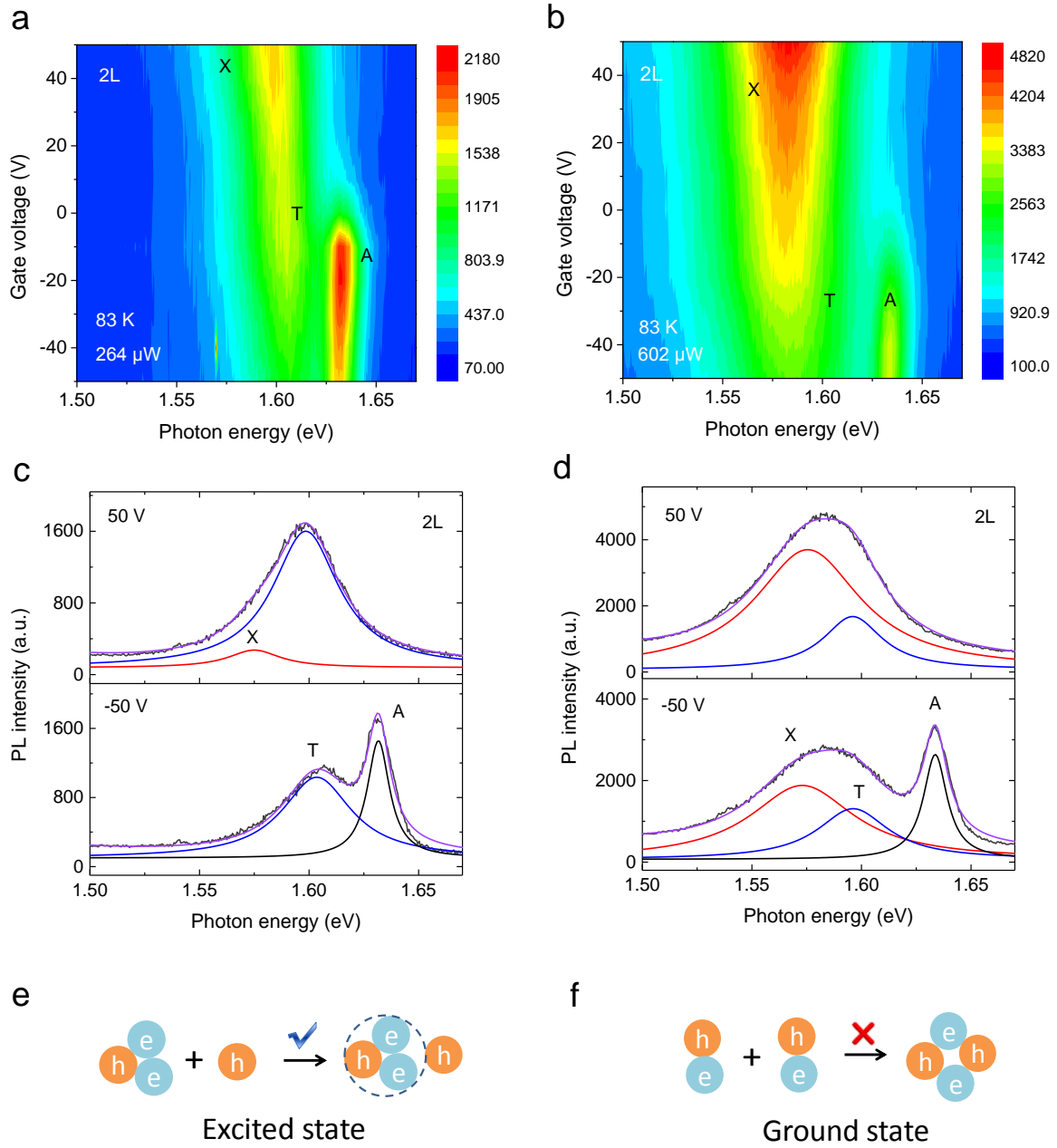


Figure 3

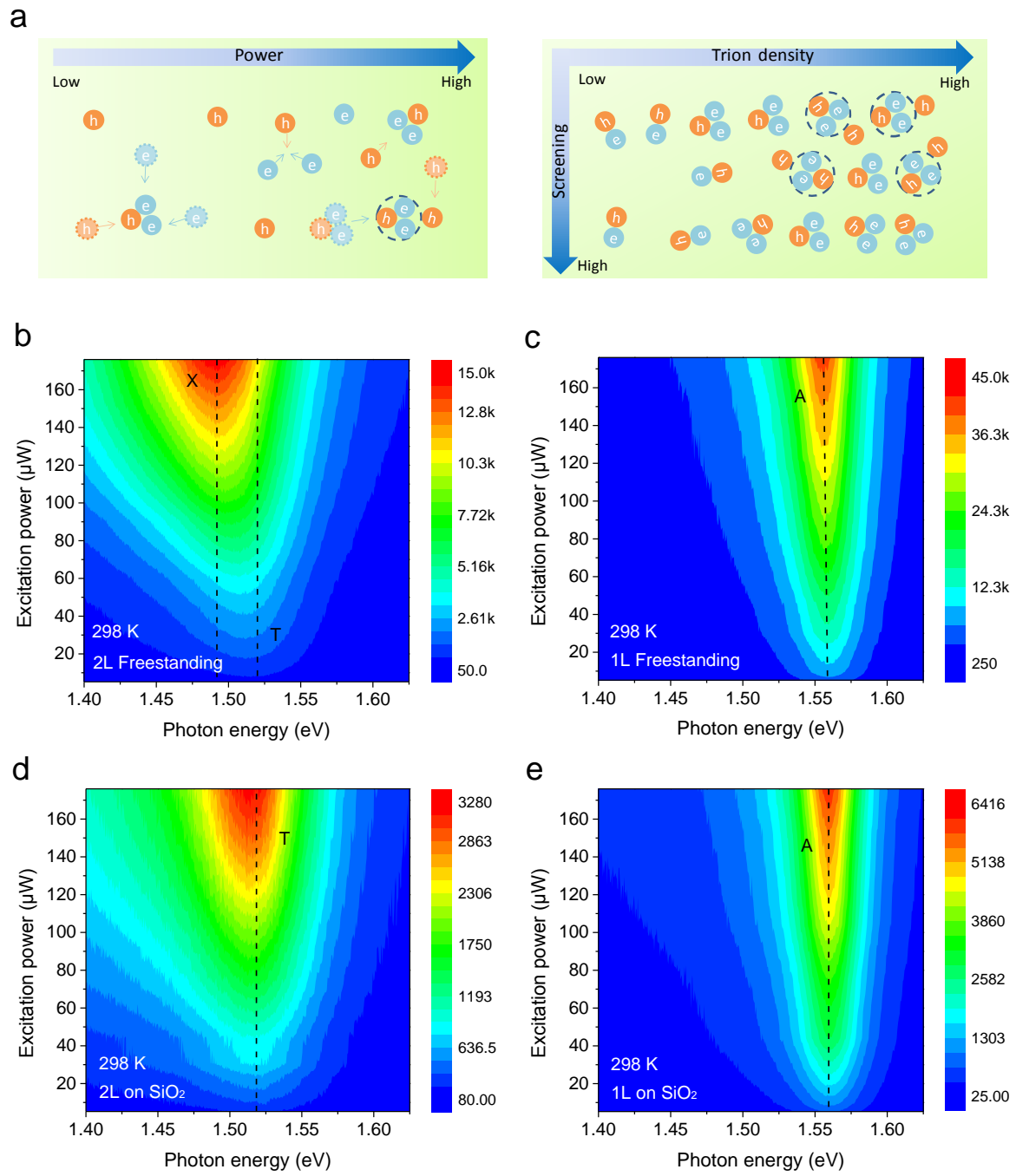


Figure 4

Table1. Measured and theoretically calculated binding energies of biexcitons in TMDs (meV).

	MoS ₂	MoSe ₂	WS ₂	WSe ₂
Theory($A+A$) ^[25]	22	18	24	20
Theory($T+C$) ^[25]	69	58	67	59
Experiments	70 ^[12]	60 ^{our}	65 ^[13]	52 ^[11]

Note: T is a trion, C is a charge and A is an exciton.

ToC graphic

